



RESEARCH ARTICLE

10.1002/2015JD024680

Key Points:

- There are significant discrepancies in reanalyses surface wind, humidity, and temperature in the Amundsen Sea area
- Temperature biases are greatest over and closer to the Antarctic continent and near the surface
- Validation data include 38 radiosondes withheld from the reanalyses

Supporting Information:

- Supporting Information S1

Correspondence to:

R. W. Jones,
Richard.W.Jones@uea.ac.uk

Citation:

Jones, R. W., I. A. Renfrew, A. Orr, B. G. M. Webber, D. M. Holland, and M. A. Lazzara (2016), Evaluation of four global reanalysis products using in situ observations in the Amundsen Sea Embayment, Antarctica, *J. Geophys. Res. Atmos.*, 121, doi:10.1002/2015JD024680.

Received 18 DEC 2015

Accepted 16 MAY 2016

Accepted article online 19 MAY 2016

Evaluation of four global reanalysis products using in situ observations in the Amundsen Sea Embayment, Antarctica

R. W. Jones¹, I. A. Renfrew¹, A. Orr², B. G. M. Webber¹, D. M. Holland³, and M. A. Lazzara^{4,5}

¹Centre of Ocean and Atmospheric Sciences, School of Environmental Sciences, University of East Anglia, Norwich, UK, ²British Antarctic Survey, Cambridge, UK, ³Courant Institute of Mathematical Sciences, New York University, New York, New York, USA, ⁴Antarctic Meteorological Research Center, Space Science and Engineering Center, University of Wisconsin-Madison, Madison, Wisconsin, USA, ⁵Department of Physical Sciences, School of Arts and Sciences, Madison Area Technical College, Madison, Wisconsin, USA

Abstract The glaciers within the Amundsen Sea Embayment (ASE), West Antarctica, are amongst the most rapidly retreating in Antarctica. Meteorological reanalysis products are widely used to help understand and simulate the processes causing this retreat. Here we provide an evaluation against observations of four of the latest global reanalysis products within the ASE region—the European Centre for Medium-Range Weather Forecasts Interim Reanalysis (ERA-I), Japanese 55-year Reanalysis (JRA-55), Climate Forecast System Reanalysis (CFSR), and Modern Era Retrospective-Analysis for Research and Applications (MERRA). The observations comprise data from four automatic weather stations (AWSs), three research vessel cruises, and a new set of 38 radiosondes all within the period 2009–2014. All four reanalyses produce 2 m temperature fields that are colder than AWS observations, with the biases varying from approximately -1.8°C (ERA-I) to -6.8°C (MERRA). Over the Amundsen Sea, spatially averaged summertime biases are between -0.4°C (JRA-55) and -2.1°C (MERRA) with notably larger cold biases close to the continent (up to -6°C) in all reanalyses. All four reanalyses underestimate near-surface wind speed at high wind speeds ($>15\text{ m s}^{-1}$) and exhibit dry biases and relatively large root-mean-square errors (RMSE) in specific humidity. A comparison to the radiosonde soundings shows that the cold, dry bias at the surface extends into the lower troposphere; here ERA-I and CFSR reanalyses provide the most accurate profiles. The reanalyses generally contain larger temperature and humidity biases, (and RMSE) when a temperature inversion is observed, and contain larger wind speed biases (~ 2 to 3 m s^{-1}), when a low-level jet is observed.

1. Introduction

The glaciers within the Amundsen Sea Embayment (ASE; see Figure 1a for location), one of the three major basins which drain the West Antarctic Ice Sheet, are amongst the most rapidly retreating in Antarctica, with this region responsible for about 10% of current global sea level rise [Mouginot *et al.*, 2014]. It is thought that this retreat is primarily driven by relatively warm circumpolar deep water being transported onto the continental shelf and driving basal melting of the ice shelves that buttress these glaciers [Pritchard *et al.*, 2012; Rignot *et al.*, 2013]. Ocean modeling and observations have revealed that large-scale zonal wind anomalies near the continental shelf break are important in controlling the variability of this melt [Thoma *et al.*, 2008; Dutrieux *et al.*, 2014]. Knowing the state of the atmosphere in the ASE over time is vital for understanding and modeling the climate processes at work here.

Meteorological reanalysis aims to provide the best estimate of the atmospheric state at any one time, by combining in situ and satellite observations with forecast model data from a fixed version of a numerical weather prediction system. Usually, reanalysis data sets provide global coverage over a period of several decades. As the ASE region is remote, and in situ meteorological observations are sparse and unevenly distributed, reanalysis products are a valuable tool for studying weather and climate. However, because oceanographic and atmospheric models can be highly sensitive to their forcing data [e.g., Condon and Renfrew, 2013], it is necessary to evaluate reanalysis data against available in situ measurements in order to determine their utility. Four of the latest generation of global reanalysis are evaluated here: the European Centre for Medium-Range Weather Forecasts (ECMWF) Interim Reanalysis (ERA-I), [see Dee *et al.*, 2011], the Japanese 55 year Reanalysis (JRA-55) [see Kobayashi *et al.*, 2015], the Climate Forecast System Reanalysis (CFSR) from the National Center for

©2016. The Authors.

This is an open access article under the terms of the Creative Commons Attribution License, which permits use, distribution and reproduction in any medium, provided the original work is properly cited.

Table 1. The Latitude, Longitude, Altitude, Mean Temperature, and Mean Pressure Recorded at Each of the Four AWS: Evans Knoll (EK), Thurston Island (TI), Bear Peninsula (BP), and New York University (NYU)

Site Details	EK	TI	BP	NYU
Longitude (°W)	100.40	97.55	111.89	100.71
Latitude (°S)	74.85	72.53	74.55	75.01
Altitude (m)	178	212	312	70
Mean temperature (°C)	−13.01	−11.21	−13.60	−15.39
Mean pressure (hPa)	962.7	954.4	930.3	975.3

atmospheric models [Deb *et al.*, 2016]. Glaciological studies such as Medley *et al.* [2014] have compared the average accumulation derived from a radar survey and firn cores with reanalysis data sets. This allows validation of their observation-based accumulation rates and as such helps to constrain surface mass balance estimates.

Despite the frequent use of reanalysis products within the ASE, there has been, to our knowledge, no comprehensive effort to validate them in this data sparse region. Bracegirdle [2013] used pressure observations from three drifting buoys released in the neighboring Bellingshausen Sea to evaluate mean sea level pressure fields from reanalysis products. The author found ERA-I had the smallest bias (~ 0.5 hPa), although both CFSR and MERRA also showed biases of less than 1 hPa. It has been shown that there are relatively large surface temperature biases over Antarctica in five global meteorological reanalysis data sets compared with automatic weather stations (AWSs) both on the interior plateau and in outlying coastal regions [see Bracegirdle and Marshall, 2012; Jones and Lister, 2015 (for ERA-I only)]. However, neither of these studies included any observations from the coastal Amundsen Sea sector nor from over the adjacent ocean.

Here we provide a comprehensive evaluation of ERA-I, MERRA, CFSR, and JRA-55 for the ASE, including PIG. We use surface observations collected from four AWSs and three research vessel cruises, as well as a new set of 38 radiosondes launched offshore during one of the oceanic cruises.

2. Data Sets and Methodology

2.1. Reanalyses

Four of the most recently released global reanalyses are evaluated in this study: ERA-I, JRA-55, CFSR, and MERRA. For ERA-I, JRA-55, and MERRA the reanalysis fields are used, while for CFSR the near-surface variables from the associated 6 h reforecast are used. (Note that after 2010 CFSR version 2 data are used, this is essentially the same model as used in the first CFSR and version 2 is being used to extend the CFSR data forward to the present day; from hereon we will refer to both products as the CFSR). The approximate grid size of the reanalysis products (at the tropics) is ~ 79 km for ERA-I (T255), ~ 55 km for JRA-55 (T319), ~ 38 km for CFSR (T382), and ~ 50 km for MERRA (0.5° by 0.67°). ERA-I and JRA-55 both have 60 vertical levels with a model top at 0.1 hPa, CFSR has 64 vertical levels with the highest level at 0.26 hPa, and MERRA has 72 vertical levels up to 0.01 hPa. All the reanalyses used here are provided at a 6 h temporal resolution.

For evaluations such as this one, it is ideal to include some observational data sets which are *not* assimilated, i.e., that are entirely independent of the reanalysis data. Our radiosonde observations were definitely not assimilated as they were deliberately withheld from the Global Telecommunications System (GTS). The ECMWF website suggests that both sea level pressure and wind speed from research vessels, and all AWS data are made available via the GTS and so could have been assimilated. In practice it is difficult to check whether every cruise or AWS data set has been assimilated.

2.2. Automatic Weather Stations

The Antarctic Meteorological Research Center (AMRC) has AWS observations from many sites around the continent. The Evans Knoll, Thurston Island, and Bear Peninsula AWSs are all located in coastal areas of the ASE, and henceforth we will refer to these as the AMRC sites (see Figure 1b and Table 1 for locations). The AMRC AWSs used here are of the CR1000 type [see Lazzara *et al.*, 2012]. They were installed in January 2011 by scientists from New York University (NYU), and our evaluation period for these sites spans 1 February 2011 to 28 February 2014. We also use data from a fourth “NYU” AWS located on PIG, again installed by scientists from NYU and moved to its present location in January 2013. At this site the evaluation period spans 1 February 2013 to 28 February 2014. Each of the AWSs records atmospheric temperature, relative humidity, wind speed, and wind direction at a nominal height of 3 m above the surface, while atmospheric pressure is measured close to the foot of the mast (see Table 1 for average conditions;

see supporting information Table S1 for instrumentation details). The observations are stored at 10 min temporal resolution, here we subsample the observations to 6-hourly temporal resolution for consistency with the reanalysis data.

All three of the AMRC sites are surrounded by complex topography, which is not fully resolved by the reanalyses. Such topography is typical for coastal regions of West Antarctica, and the AWS sites are thus representative. The AMRC AWSs were installed on nunataks (rock outcrops). The NYU AWS is located on PIG, and the surrounding topography of the glacier is relatively uniform.

AWSs in Antarctica are prone to overestimate temperature during low-wind speed conditions due to a lack of ventilation [Genthon *et al.*, 2011; Lazzara *et al.*, 2012], particularly in austral summer when there is near 24 h daylight. To mitigate this error, low-wind speed periods (less than 2 m s^{-1}) are removed from the summertime temperature comparison (approximately 20% of the summertime data). Note that at the Bear Peninsula AWS, the anemometer stopped working during 2013 so the wind comparison there is based on only 2 years of data.

2.3. Research Vessels

The research vessel meteorological data are from the RRS *James Clark Ross* (*JCR*), the RV *Polarstern* [see König-Langlo, 2010], and the *Nathaniel B. Palmer* [see Jacobs, 2014]. Observations of temperature, wind, humidity, and pressure are used here (see Table S1 for details). Instruments on board the *JCR* were calibrated against national standards, and we understand similar checks were carried out for the *Polarstern* and *Palmer* instruments. Each ship was within the ASE for approximately 1 month, the *JCR* in February–March 2014, the *Polarstern* in March 2010, and the *Palmer* in January–February 2009. Across the three research cruises there is approximately 3 months of data at 6-hourly resolution.

The sea ice conditions differed somewhat between the three cruises. In 2009 when the *Palmer* was in the ASE the reanalysis products all show a high concentration of sea ice at the continental shelf break (see Figure 1b for shelf break location), extending to approximately 73°S and lower concentrations closer to PIG and Thwaites. In March 2010 while the *Polarstern* was in the region, there was a high concentration of sea ice to the west of the region shown in Figure 1b (120°W and 110°W) but lower concentrations close to PIG and Thwaites glacier. In February 2014 while the *JCR* was in the region, sea ice concentrations were generally low but with an area of high concentration to the north of Thurston Island (see Figure 1b for mean concentration).

2.4. Radiosondes

A set of 38 radiosondes were successfully launched between 1 February and 4 March 2014 during the *JCR* cruise (see Figure 1b for locations). The radiosondes were RS92 Väisälä sondes, measuring temperature, humidity, and pressure with winds calculated using Global Positioning System (GPS). The RS92 Väisälä radiosondes have been shown to provide more accurate measurements of relative humidity at low temperatures than previous generation Väisälä sondes (RS90 and RS80) [Suortti *et al.*, 2008]. The variables are recorded every 2 s ($\sim 10 \text{ m}$ intervals) during the ascent. Typically, the radiosondes reached a maximum altitude of approximately 20 km, well above the tropopause. Usually, there was one radiosonde launched each day at around 1200 UTC (see Table S2 for details). On three days (13, 18, and 23 February 2014) several sondes were launched to investigate particular weather events. The radiosonde profiles have been checked for consistency both with surface observations, and within each profile and no calibration errors are found. In three of the profiles no wind data was recorded due to a problem with the GPS communications system. As noted above, these radiosonde observations were deliberately withheld from the GTS, and hence the reanalyses, in order to provide independent observations in the ASE.

2.5. Methodology

To allow comparison between the observations and gridded reanalysis data sets, an appropriate methodology must be chosen. In the AWS comparison the nearest land grid point is used. For the ship and radiosonde data we use the nearest reanalysis grid point for the comparison. Due to the smoothed topography of the reanalyses, resulting in the seaward extension of the land sea mask in the ASE, a comparison to the nearest marine grid point is troublesome, as this can be $\sim 100 \text{ km}$ distant. Instead, we used the nearest grid point which does mean that on some occasions land grid points are used.

For the AWS data we focus our comparison on temperature, humidity, wind speed, and wind direction. Reanalysis wind speed and direction are available at 10 m above the surface, and temperature and humidity fields at 2 m. In the AWS comparison, given the uncertainty of the observation height due to snow accumulation, the 2 m reanalysis fields are directly compared to the AWS temperature and humidity observations (recorded at a nominal height of 3 m above the surface). A height adjustment is applied to the 10 m reanalysis wind speed to 3 m, assuming a logarithmic wind profile with a roughness length of 0.1 mm (appropriate for snow) and neutral atmospheric stability—similar to *Bromwich et al.* [2013]. This simple adjustment is used as the atmospheric stability is unknown from the AWS observations.

It is also necessary to adjust the reanalysis temperatures for the difference in height between the grid point and the AWS. Failure to adjust temperatures in this way can result in spurious temperature biases [*Bracegirdle and Marshall*, 2012]. Due to the climatologically cold and dry Antarctic atmosphere, we adjusted the reanalysis temperatures to the listed altitude of each AWS using the dry adiabatic lapse rate of $9.8^{\circ}\text{C km}^{-1}$. The same $9.8^{\circ}\text{C km}^{-1}$ adjustment was made by *Bracegirdle and Marshall* [2012], although *Jones and Lister* [2015] used the moist lapse rate of $6^{\circ}\text{C km}^{-1}$. Due to the presence of surface-based temperature inversions and the often steep coastal topography, the lapse rate is likely to be highly variable, so the use of a constant lapse rate is an approximation. As an example of the size of this approximation, the height of the ERA-I grid point at Evans Knoll is 260 m, 82 m higher than the AWS height. Using the dry adiabatic lapse rate the ERA-I temperatures are adjusted by $+0.8^{\circ}\text{C}$, whereas, if the $6^{\circ}\text{C km}^{-1}$ lapse rate was used the adjustment would be $+0.5^{\circ}\text{C}$. These differences are an order of magnitude smaller than the most significant biases discussed later. The AWSs at Bear Peninsula, Thurston Island, and on PIG (NYU) are colocated with University NAVSTAR Consortium GPS stations, and as such we have some confidence in their listed elevation. However, if the AWS altitudes are incorrectly listed, by, e.g., 50 m, the temperature biases described later would change by $\sim 0.5^{\circ}\text{C}$, the error in the listed elevation is unlikely to be larger than this. Table 1 shows the location and listed altitude of each AWS alongside the mean observed temperature and pressure.

The research vessel observations are recorded at heights between 19 and 37 m above the sea surface and are adjusted to 10 m or 2 m for comparison with the reanalysis products. In order to do this the observed sea surface and atmospheric temperatures are used to calculate atmospheric stability, and then a height adjustment based on Monin-Obukhov similarity theory is made (e.g., following *Smith* [1988] or *Renfrew et al.* [2002]).

In the radiosonde comparison both the observations and reanalysis pressure-level data are interpolated onto a 5 hPa vertical grid. The focus here is on the lower troposphere, so the comparison is limited to between the surface and 800 hPa (approximately 2 km altitude). Note also that the JRA-55 has a reduced horizontal resolution (1.5° by 1.5°) for its pressure-level data.

3. Results

3.1. Comparison With AWS Observations

The representation of 2 m temperature is evaluated by season due to the large differences between summer and winter insolation in the Antarctic, which result in significant seasonal variations in temperature. During winter the absence of insolation allows longwave radiative cooling of the surface to dominate, generally resulting in the formation of a strongly stable, cold boundary layer [*King*, 1990]. In summer the boundary layer is warmer and tends to be weakly stably stratified or even slightly unstable [*Mastrantonio et al.*, 1999].

As an example the seasonal temperature biases from the Bear Peninsula AWS are shown in Figure 2. At Bear Peninsula (and across the other AMRC sites) ERA-I records its smallest bias in the austral summer and its largest bias in the austral winter (Figure 2). MERRA has large biases across all seasons (Figure 2). Table 2 shows that across the AMRC sites both ERA-I and JRA-55 show a marked improvement in reproducing 2 m temperatures in summertime. Summertime biases for ERA-I and JRA-55, respectively, are -0.23°C and -1.91°C , compared with -3.70°C (ERA-I) and -3.89°C (JRA-55) wintertime biases. This suggests that ERA-I and JRA-55 have more skill at capturing the weakly stable or even unstable summer boundary layer, whereas the CFSR and MERRA temperature biases show little seasonal variability.

Table 2 also shows that the mean 2 m temperature biases at the AMRC sites are negative during all seasons, for all the four reanalysis products. The weighted (by length of time series) mean annual bias for all four sites shows that ERA-I has the smallest bias (-1.81°C), compared with CFSR (-2.50°C), JRA-55 (-2.62°C), and

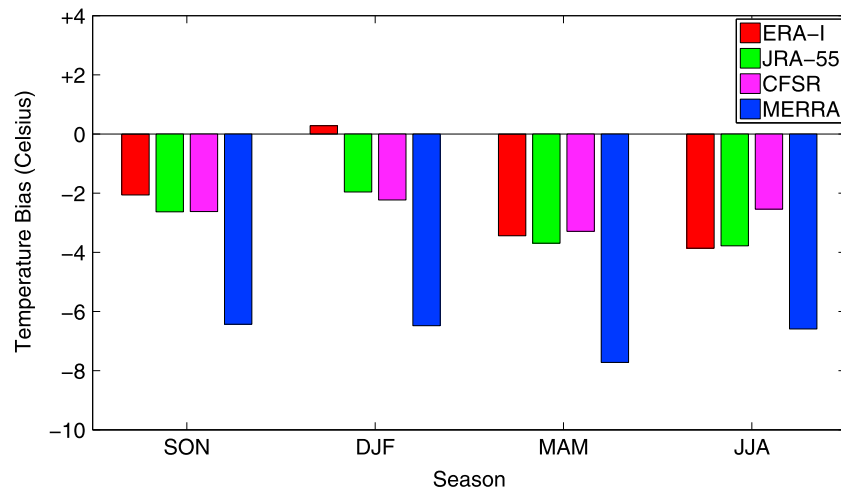


Figure 2. The magnitude of seasonal temperature biases for each of the reanalysis products at the Bear Peninsula AWS.

MERRA (−6.80°C). For MERRA the bias is significantly greater than the −1.6°C average bias found at coastal East Antarctic stations by *Bracegirdle and Marshall* [2012], suggesting MERRA may have a very strong regional bias in West Antarctica.

Jones and Lister [2015] using ERA-I show that 2 m temperatures are cold biased compared with a group of AWS on the Ross Sea coastline and three sites on the western side of the Antarctic Peninsula by between −1.1 and −2.4°C (for 2002–2013 period). Although at two sites on the Ross Sea (Cape Ross and Arelis), *Jones and Lister* [2015] find small positive biases for the same period. Here individual site biases range from −2.98°C at Thurston Island to +1.9°C at NYU, with three of the four sites showing cold biases of −1.5 to −3.0°C.

Table 2. A Comparison of 2 m Temperatures From Reanalyses to Observed AWS Temperatures^a

Product	Stats	AMRC 3 Site Average				NYU ^b				Annual Average Bias
		SON	DJF	MAM	JJA	SON	DJF	MAM	JJA	
ERA-I	Bias	−2.27	−0.23	−2.66	−3.70	1.35	0.36	3.02	2.83	−1.80
	SD Ratio	1.17	1.09	1.29	1.25	0.88	0.90	0.97	0.95	
	R ²	0.79	0.72	0.74	0.73	0.93	0.83	0.88	0.86	
	RMSE	4.37	2.22	5.16	6.34	2.83	2.06	4.44	4.32	
	Slope	1.04	0.93	1.12	1.07	0.85	0.82	0.91	0.89	
JRA-55	Bias	−2.82	−1.91	−3.40	−3.89	0.07	−0.18	1.74	1.55	−2.62
	SD Ratio	1.01	1.14	1.03	0.92	0.81	0.84	0.82	0.74	
	R ²	0.82	0.74	0.80	0.80	0.83	0.69	0.84	0.76	
	RMSE	4.17	2.88	4.68	5.29	3.74	2.70	4.24	4.77	
	Slope	0.91	0.98	0.92	0.82	0.74	0.70	0.75	0.64	
CFSR	Bias	−2.88	−2.63	−2.96	−2.68	−0.48	−2.50	1.52	1.79	−2.50
	SD Ratio	1.20	1.37	1.26	1.18	1.04	1.29	1.00	1.06	
	R ²	0.75	0.62	0.75	0.73	0.78	0.59	0.84	0.79	
	RMSE	5.02	4.02	5.19	5.45	4.31	4.75	4.13	4.71	
	Slope	1.04	1.08	1.09	1.01	0.92	0.99	0.92	0.94	
MERRA	Bias	−6.62	−6.86	−7.87	−6.89	−4.57	−6.00	−4.21	−3.11	−6.80
	SD Ratio	1.06	1.28	1.12	0.99	0.95	1.04	1.01	0.98	
	R ²	0.82	0.73	0.79	0.80	0.85	0.75	0.83	0.81	
	RMSE	7.31	7.29	8.57	7.72	5.69	6.52	5.78	4.94	
	Slope	0.96	1.09	1.00	0.89	0.88	0.90	0.92	0.88	

^aA negative bias indicates that the reanalysis product is colder than the observations. SON, DJF, MAM, and JJA indicate the season. The standard deviation ratio (SD ratio) is the standard deviation of the reanalyses divided by that observed. R² has its standard statistical meaning as a measure of the correlation. RMSE is the root-mean-square error. Slope indicates the gradient of the linear regression line. The unit for bias and RMSE is degrees Celsius. The AMRC site average is calculated from the Evans Knoll, Thurston Island, and Bear Peninsula AWS sites. The right-hand column shows the weighted mean annual bias across the four sites. SON, September–October–November; DJF, December–January–February; MAM, March–April–May; and JJA, June–July–August.

^bThe NYU data set only covers a 13 month period.

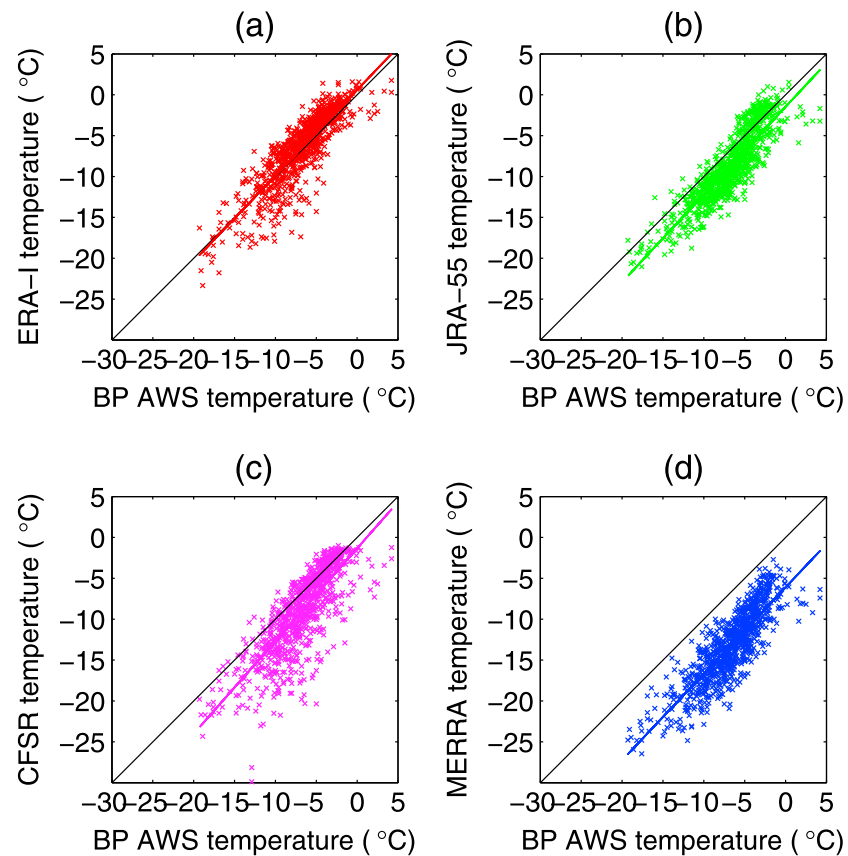


Figure 3. Scatterplots showing the Bear Peninsula (BP) AWS observed summertime temperature (2011–2014) against the 2 m temperatures from the reanalyses: (a) ERA-I, (b) JRA-55, (c) CFSR, and (d) MERRA.

These combined results are suggestive of a systematic cold bias in ERA-I 2 m temperatures (of approximately -1.5°C) extending around West Antarctica from the Ross Sea to the Antarctic Peninsula.

The NYU AWS—located near the middle of the floating portion of PIG and at relatively low altitude—is notably different with positive biases in the ERA-I, JRA-55, and CFSR reanalyses (Table 2). The linear regression slope values are all less than 1 due to a warm bias at low temperatures (not shown). The NYU AWS is the only one located on an ice shelf and so may be more prevalent to cold-air drainage during katabatic flows—a phenomena that is difficult to properly model [e.g., Renfrew, 2004], leading to a warm bias. MERRA remains colder than observations at the NYU AWS, although the magnitude of the bias is smaller than that at the AMRC sites.

As an illustration of the summertime temperature comparisons, Figure 3 shows scatterplots for the Bear Peninsula site which are representative of all the AMRC sites. The CFSR comparison (Figure 3c) shows more scatter than the other products and consequently has a relatively large root-mean square error (RMSE) and a reduced R^2 (correlation coefficient) value of 0.63, compared with 0.72 (MERRA), 0.74 (ERA-I), and 0.77 (JRA-55). Both CFSR and ERA-I tend to have larger RMSEs when observed summertime temperatures fall below -10°C . Furthermore, CFSR and MERRA tend to produce a larger range of summertime temperatures than observed, due to their anomalously cold temperatures, which leads to standard deviations that are larger than observed (Table 2). The bias in the MERRA comparison is noticeably larger than for the other reanalyses.

Wind speed and humidity comparison statistics can be found in Table 3. For brevity we show annual averages here as the seasonal differences are negligible. All of the reanalysis products are biased low in wind speed and struggle to reproduce the observed spread of wind speeds as indicated by standard deviation ratios of between 0.43 and 0.81. Figure 4 shows example scatterplots for the Thurston Island site, which is also representative of the other sites. The reanalyses tend to overestimate the strength of the wind when

Table 3. A Comparison of the Four Reanalysis Products Across the Four AWS Sites for Wind Speed, Relative Humidity, and Specific Humidity Average Over All Seasons^a

Product	Stats	Wind Speed (m s^{-1})		Relative Humidity (%)	Specific Humidity (g kg^{-1})
		AMRC	NYU	AMRC	AMRC
ERA-I	Bias	-1.32	-0.80	-5.20	-0.20
	SD Ratio	0.53	0.72	0.87	1.06
	R^2	0.43	0.63	0.25	0.87
	RMSE	5.73	3.22	14.12	0.39
	Slope	0.34	0.57	0.43	0.99
JRA-55	Bias	-0.58	-0.63	5.46	-0.25
	SD Ratio	0.61	0.81	0.66	1.03
	R^2	0.46	0.75	0.36	0.81
	RMSE	5.31	2.66	12.99	0.47
	Slope	0.42	0.70	0.37	0.92
CFSR	Bias	-1.85	-2.27	12.33	-0.05
	SD Ratio	0.54	0.57	0.47	1.12
	R^2	0.45	0.71	0.27	0.85
	RMSE	5.46	3.83	17.22	0.38
	Slope	0.36	0.48	0.23	1.04
MERRA	Bias	-0.40	-1.55		-0.63
	SD Ratio	0.43	0.68		0.74
	R^2	0.37	0.60		0.79
	RMSE	5.62	3.61		0.76
	Slope	0.32	0.53		0.65

^aThe statistics are the same as those in Table 2. Note that humidity is not available at the NYU site.

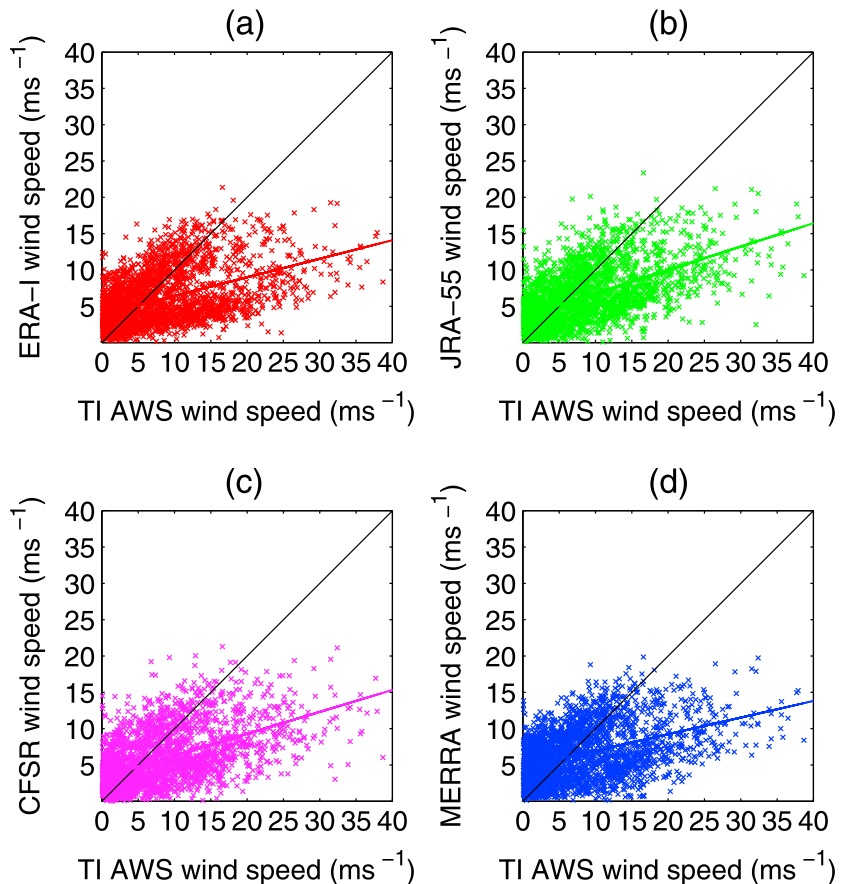


Figure 4. Scatterplots showing the Thurston Island (TI) AWS observed wind speed (2011–2014) against the neutrally adjusted 3 m wind speed from the reanalyses: (a) ERA-I, (b) JRA-55, (c) CFSR, and (d) MERRA.

Table 4. A Comparison of the Four Reanalysis Products to Meteorological Data From Three Research Vessel Cruises to the Amundsen Sea; *RRS James Clark Ross* (Feb 2014), the *Polarstern* (March 2010), and the *Palmer* (January–February 2009)^a

Product	Stats	Pressure (hPa)	Temperature (°C)	Wind Speed (m s ⁻¹)	Specific Humidity (g kg ⁻¹)	Relative Humidity (%)
ERA-I	Bias	0.00	-0.62	-0.82	-0.20	-3.73
	SD Ratio	1.00	1.20	0.97	1.08	1.03
	R ²	0.99	0.77	0.48	0.84	0.54
	RMSE	0.74	1.64	3.00	0.34	7.78
	Slope	1.00	1.04	0.67	0.99	0.77
JRA-55	Bias	-0.05	-0.39	-0.32	-0.03	2.03
	SD Ratio	1.01	1.22	0.96	1.11	0.84
	R ²	0.99	0.76	0.71	0.79	0.48
	RMSE	1.26	1.58	1.96	0.32	7.53
	Slope	1.00	1.04	0.81	0.97	0.59
CFSR	Bias	-0.22	-1.63	-0.83	-0.22	2.32
	SD Ratio	1.01	1.55	0.81	1.15	0.65
	R ²	0.97	0.72	0.46	0.83	0.34
	RMSE	1.85	2.88	2.88	0.39	8.66
	Slope	0.99	1.28	0.55	1.04	0.37
MERRA	Bias	0.46	-2.08	-1.02	-0.30	1.02
	SD Ratio	1.01	1.50	0.81	1.11	0.80
	R ²	0.98	0.60	0.62	0.71	0.26
	RMSE	1.46	3.38	2.46	0.51	9.10
	Slope	1.00	1.13	0.64	0.93	0.39

^aObservational data are corrected from sensor height to reanalysis output height.

the observed wind speed is low (<5 m s⁻¹) and severely underestimate the strength of the wind when the observed wind speed is high (>15 m s⁻¹). Across the AMRC sites the combination of these errors at low and high wind speeds causes the linear regression slopes to be very low, between 0.3 and 0.45 for all reanalysis products, compared to the ideal of 1 (Table 3 and Figure 4). The performance at the NYU AWS site is similar, with all products showing a low slope and a negative bias. The reanalysis products represent low wind speeds better at NYU (not shown), leading to an improvement in the slope and correlation values there.

Analysis of strong wind events (>15 m s⁻¹) at Thurston Island and Bear Peninsula revealed that at both sites the wind direction was from a north or north easterly direction during >75% of these events (not shown). This suggests there may be an enhancement of the observed winds due to flow distortion, particularly at Thurston Island with mountainous terrain to the north (see Figure 1b). Such flow distortion is poorly represented in models with insufficient resolution [e.g., Renfrew *et al.*, 2009; Elvidge *et al.*, 2016]. The northerly wind direction suggests that such winds are associated with synoptic-scale cyclones located offshore. Models with a coarser horizontal resolution have been shown to contain larger wind speed biases during Antarctic strong wind event where a cyclone and topographic effects combine to produce the strongest winds [Turner *et al.*, 2009; Orr *et al.*, 2014].

The biases in the 2 m relative humidity (RH) field vary from -5.2% for ERA-I to 12.33% for CFSR (Table 3). RMSE ranges from 13% (JRA-55) to 17% (CFSR) at the AMRC sites. It is, however, notoriously difficult to measure RH particularly in the harsh environment in which these AWSs are located, and problems with the observations may contribute to RH biases and RMSE [Renfrew and Anderson, 2002]. Due to the low observed temperatures the specific humidity is low, averaged across the AMRC sites the mean value is 1.42 g kg⁻¹. CFSR has the smallest dry bias in the specific humidity field of 0.05 g kg⁻¹. MERRA is drier than observed by 0.63 g kg⁻¹, ERA-I and JRA-55 produce dry biases of ~0.2 g kg⁻¹.

3.2. Comparison With Research Vessel Observations

Summertime research vessel cruises to the Amundsen Sea have become frequent in recent years with several visits since 2007 [Dutrieux *et al.*, 2014]. Here we utilize research vessel meteorological data from three cruises (Table 4).

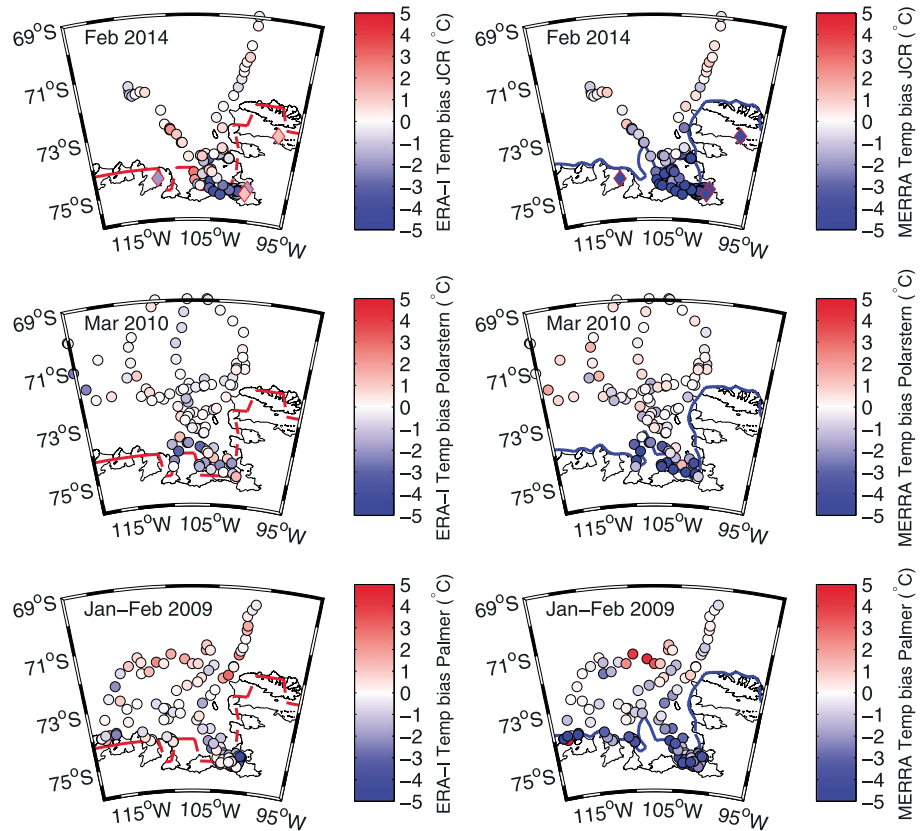


Figure 5. Spatial variability of reanalysis temperature biases (left column, ERA-I; right column, MERRA) in comparison to ship meteorological data from: (top row) *RRS JCR*, (middle row) the *Polarstern*, and (bottom row) *Palmer*. In the *JCR* figures the mean temperature bias from AWS for the month of February 2014 is shown in diamonds with red edge color. The dashed lines show the land sea mask (here the 0.95 contour is shown for ERA-I and 0.5 contour for MERRA).

Pressure is extremely well represented by all the reanalyses; the magnitude of biases in mean sea level pressure is less than 0.5 hPa, and the R^2 values are greater than 0.95 (Table 4). *Bracegirdle* [2013] found pressure biases of similar magnitude using drifting buoys in the neighboring Bellingshausen Sea.

As seen in the AWS comparison, all four products show colder temperatures than those observed, with MERRA showing the largest average bias of -2.08°C . Similar to the AWS comparison, ERA-I and JRA-55 display a smaller (summertime) temperature bias than CFSR (Table 4). Figure 5 shows the spatial distribution of temperature biases for ERA-I and MERRA. In both products there is a tendency for temperature biases to be most negative closer to the coastline (with the largest biases approaching -6°C), this is also true of CFSR and JRA-55 (not shown). For MERRA the negative temperature bias is particularly clear in the *JCR* and *Palmer* comparisons as these cruises spent more time close to PIG ice shelf. The temperature biases for the AWS sites corroborate the research vessel comparison, as illustrated in Figure 5 (top row).

The reanalysis products underestimate the mean wind speed compared to the ship observations by between -0.32 m s^{-1} (JRA-55) and -1.02 m s^{-1} (MERRA). There is no clear pattern of spatial variability in the wind speed bias for any of the reanalysis products, as illustrated for JRA-55 in Figure 6. Scatterplots for all three cruises (not shown) indicate an improved representation of high wind speeds than seen in the AWS comparison. The biases even at wind speeds between 15 and 19 m s^{-1} (the highest observed ship wind speeds) are small. Pressure and wind speed observations from the research vessels are made available for assimilation into the reanalyses, and this may be partly why the bias is reduced. In contrast to the results seen here, *Li et al.* [2013] have shown that ERA-I contains biases at low and high wind speeds compared with Southern Ocean ship observations, overestimating low winds and underestimating high winds. Here we see little evidence of such systematic biases but note that our sample is limited, there are few strong wind observations from the research vessels in the Amundsen Sea.

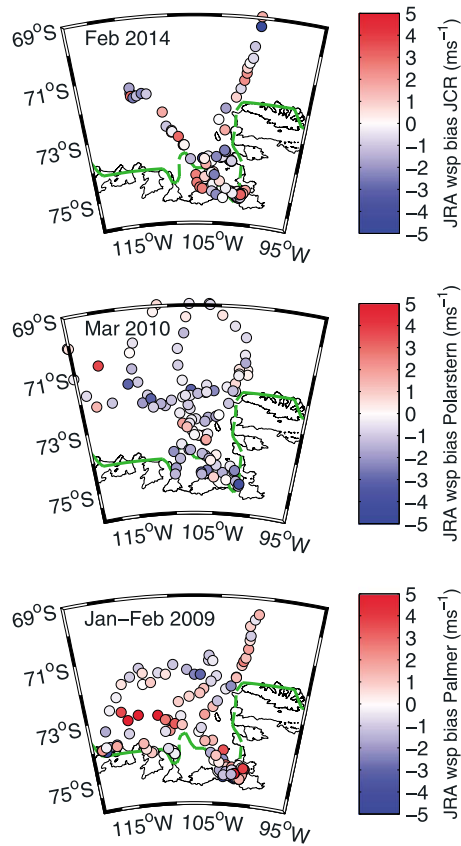


Figure 6. Spatial variability of wind speed biases for JRA-55 in comparison to ship meteorological data from: (top) *RRS JCR*, (middle) the *Polarstern*, and (bottom) *Palmer*. The dashed lines show land sea mask in each of the products (here the 0.5 contour is shown for JRA-55).

JRA-55 also produces a similar shaped mean profile compared with the observations but has a larger bias of between -1 and -2°C . In the boundary layer MERRA has a large cold bias: at 975 hPa the average MERRA temperature is 4°C colder than the observations, consistent with the large near-surface biases observed during the *JCR* cruise (Figure 5 and Table 4).

All four of the reanalyses produce similar mean wind speed profiles (Figure 7c). At 975 hPa they all accurately reproduce near-surface wind speed to within 1 m s^{-1} . Above this the observations show a distinct low-level jet (discussed later) which is not captured by the reanalyses. As such there is a negative bias for all of the products, with average wind speeds $\sim 2\text{ m s}^{-1}$ lower than the observations between 950 and 850 hPa.

The specific (Figure 7b) and relative humidity (Figure 7d) mean profiles reveal that ERA-I and CFSR provide accurate profiles of atmospheric moisture; ERA-I is perhaps the most accurate, particularly in the relative humidity profile. MERRA and JRA-55 are both drier than the observations, although JRA-55 accurately produces the relative humidity profile between 975 and 920 hPa, with larger biases above this. The specific humidity profile shows a significant dry bias of 0.5 g kg^{-1} for MERRA between 975 hPa and 925 hPa, which reduces with increasing height. This is linked to the MERRA cold bias, colder air can hold less moisture, and as such there is a dry bias in the same part of the profile as the cold bias. *Jakobson et al.* [2012] also find that MERRA is drier than observations of both specific and relative humidity in the Arctic, which suggests that MERRA may have difficulties with moisture budgets or transport near Arctic sea ice and continental shelf regions of Antarctica.

By splitting the radiosondes into two groups by location (see Figure 1b), it becomes clear that the temperature biases seen in Figure 7 are, in the main, caused by the group of radiosondes launched closer to the

Biases in the specific and relative humidity fields are generally slightly smaller than those seen in comparison to summertime AWS observations (not shown). The spatial distribution of biases (not shown) reveals that there is a tendency for larger dry biases in the specific humidity fields of MERRA and CFSR close to the coastline. This is spatially coherent with low-temperature biases observed in the same region (see Figure 5). As MERRA and CFSR both give temperatures that are too cold, they are also likely to have too little moisture. In the other reanalysis products there are no clear spatial patterns in the humidity biases; large biases are seen in many different locations for relative humidity in particular.

3.3. Comparison With Radiosonde Data

A set of 38 radiosondes was launched in the Amundsen Sea from the *JCR* cruise during February and March 2014. Having been deliberately withheld from the reanalyses they provide a unique observational data set for validating reanalysis products in this region. Here we focus on a comparison between 975 and 800 hPa, as the lower troposphere is most important for the underlying ocean and glaciers.

All of the reanalysis products have a mean temperature profile colder than the radiosondes; the 975–800 hPa mean temperature bias varies between -0.54°C for ERA-I and -1.22°C for JRA-55 (Table 5). This cold bias is consistent in sign with the research vessel near-surface temperature biases (e.g., Figure 5). The mean temperature profiles in Figure 7a show that CFSR and ERA-I mean temperatures are accurate to within $\sim 1^\circ\text{C}$ of the average radiosonde temperature from 975 hPa to 800 hPa. JRA-

Table 5. Mean Profile Statistics From 975 hPa to 800 hPa for Each of the Reanalysis Products for Temperature (Temp) (°C), Relative Humidity (%), Specific Humidity (g kg⁻¹), and Wind Speed (m s⁻¹)^a

		ERA-I		JRA-55		CFSR		MERRA	
		Bias	RMSE	Bias	RMSE	Bias	RMSE	Bias	RMSE
Temperature	All (38)	-0.54	1.42	-1.22	1.88	-0.79	1.96	-1.19	2.03
	Shelf Break (11)	0.11	1.27	-0.28	1.21	0.47	1.68	-0.31	1.47
	Continental (27)	-0.80	1.46	-1.60	2.06	-1.29	2.06	-1.50	2.13
	Inversion (16)	-0.54	1.64	-1.64	2.26	-1.02	2.19	-1.52	2.18
	Noninv (22)	-0.55	1.21	-0.92	1.54	-0.62	1.77	-0.93	1.88
Relative humidity	All	-1.22	12.47	-3.53	16.07	2.53	11.80	-7.67	17.59
	Inversion (16)	-2.68	13.09	-3.96	15.48	2.03	11.59	-10.63	19.31
	Noninv (22)	-0.16	11.82	-3.21	16.33	2.88	11.83	-5.48	15.98
Specific humidity	All	-0.05	0.24	-0.16	0.33	-0.02	0.29	-0.23	0.38
	Inversion (16)	-0.08	0.26	-0.19	0.36	-0.05	0.24	-0.31	0.43
	Noninv (22)	-0.02	0.22	-0.13	0.31	0.00	0.32	-0.17	0.32
Wind speed	All	-0.95	3.48	-1.22	3.40	-1.16	3.27	-0.75	3.30
	LLJ (21)	-1.17	3.65	-1.75	3.67	-1.75	3.40	-1.26	3.55
	Non-LLJ (17)	-0.61	3.18	-0.43	2.89	-0.29	3.03	-0.01	2.85

^aAlong with the mean of all profiles (All), the profiles have been split into groups as follows: shelf break and continental, inversion and noninversion, and low level jet (LLJ) and nonlow level jet (non-LLJ). The number of soundings in each group is noted in column 2.

Antarctic continent (Figure 8 and Table 5). All of the reanalyses have a much larger mean temperature bias for the “continental” profiles than for the “shelf break” radiosondes, with JRA-55 and MERRA producing the largest mean (975–800 hPa) biases of -1.60°C and -1.50°C, respectively. For MERRA the negative temperature bias between 975 and 900 hPa only occurs for the continental profiles, consistent with the distribution of surface biases in comparison with ship observations (Figure 5). In the layer between 975 hPa and 940 hPa, the lowest few hundred meters of the atmosphere, the MERRA mean temperature in the continental group is 4.23°C colder than that of the radiosondes.

The wind speed profiles have also been split into two distinct groups: those containing a low-level jet (LLJ) and those without (Figure 9). A LLJ in its most simplistic form is a wind speed maximum in the lower part of the atmosphere. In order to identify LLJs the definition from *Stull* [1988], and later modified by *Andreas et al.* [2000], is used. Namely, to be classified as a LLJ, a wind speed maxima must occur in the lowest 1.5 km of the atmosphere and must be at least 2 m s⁻¹ faster than both the wind speed minimum above it and the wind speed recorded at the surface. LLJs were observed in 21 of the 38 radiosonde soundings (see Figure 1b for locations).

Figure 9 shows that in the group of soundings where an LLJ is *not* observed, all the reanalysis products accurately simulate the wind speed profile between 975 and 900 hPa. Above this they tend to underestimate wind speed by between 1 and 2 m s⁻¹. When there is a LLJ, the reanalysis products (on average) show positive wind shear between 975 and 925 hPa, which indicates that at least some of the LLJs are being captured. However, they all underestimate the jet wind speed by ~2 m s⁻¹, which indicates they are either failing to produce the maximum wind speed within the LLJs or they underestimate the frequency of LLJs; inspection of individual profiles reveals that both are factors. In comparison to Arctic dropsonde data, it has been shown that ERA-I tends to produce LLJs that are both too broad and too weak [*Liu et al.*, 2015]. The mean profiles in *Liu et al.* [2015] are similar to those seen here, with ERA-I managing to reproduce wind speed maxima at approximately the same altitude as the observations but unable to reproduce the magnitudes observed. Normalized bias profiles (not shown) indicate that the bias relative to the mean observed wind speed is greater in the LLJ group than in the non-LLJ group, i.e., the reanalyses perform worse when there is a LLJ.

The radiosonde profiles have also been split on the basis of whether or not they contain a low-level temperature inversion (see Table 5). Here a temperature inversion is defined as a temperature increase of > 2°C (between the base and top of the inversion) within the profile between 975 and 800 hPa. The JRA-55, CFSR, and MERRA reanalyses all have significantly larger biases in the group of profiles when there is a temperature inversion. This larger bias is particularly apparent in the layer between 975 and 875 hPa where almost all of the temperature inversions were observed (not shown). Given that the vertical depth of

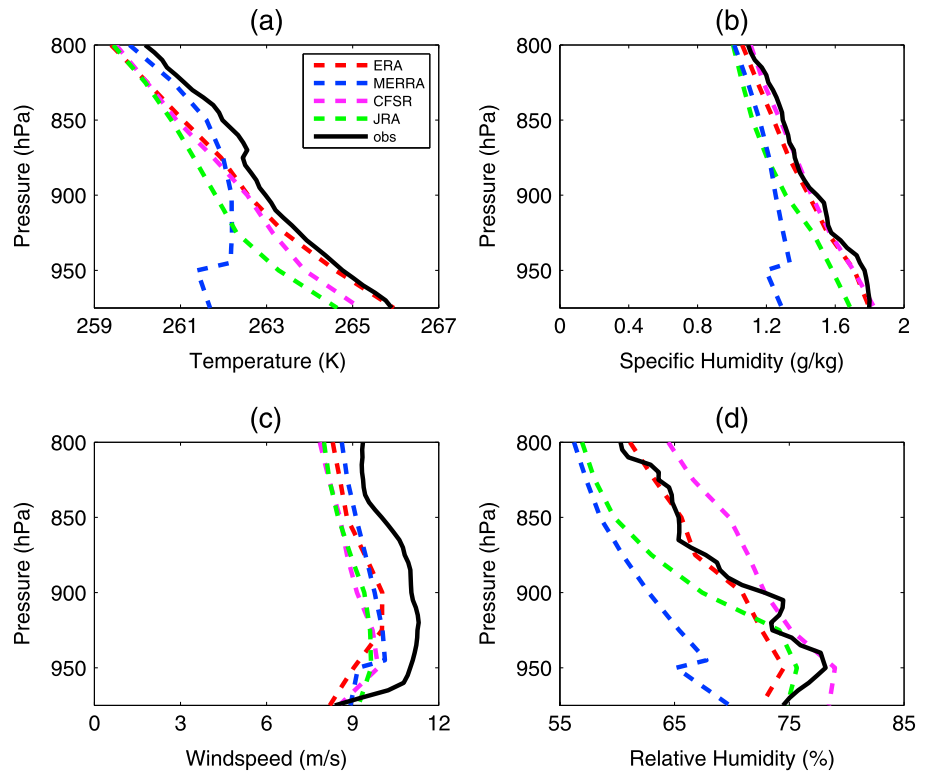


Figure 7. Mean atmospheric profiles from the radiosondes (1 February 2014 to 4 March 2014) and reanalyses: (a) temperature, (b) specific humidity, (c) wind speed, and (d) relative humidity. The colored lines represent the same reanalysis products as in Figure 2: red, ERA-I; green, JRA-55; magenta, CFSR; and blue, MERRA. Radiosonde observations are shown by the black line.

temperature inversions in the observations is typically hundreds of meters, the coarse vertical resolution of reanalysis products will struggle to capture this feature. ERA-I has a similar magnitude temperature bias in both groups, although larger RMSE in the inversion group. In the inversion group both MERRA and JRA-55 also contain larger specific humidity biases, while MERRA also has a larger RH bias (Table 5). For MERRA it seems that the additional bias is driven by a larger dry bias between 975 and 900 hPa. However, in JRA-55 the increased bias is due to the layer between 900 and 800 hPa, which is typically above the height of temperature inversions. In the Arctic multiple studies have found similar problems with the strength and depth of temperature inversions in reanalysis products [Lüpkes *et al.*, 2010; Pavelsky *et al.*, 2010; Harden *et al.*, 2011;

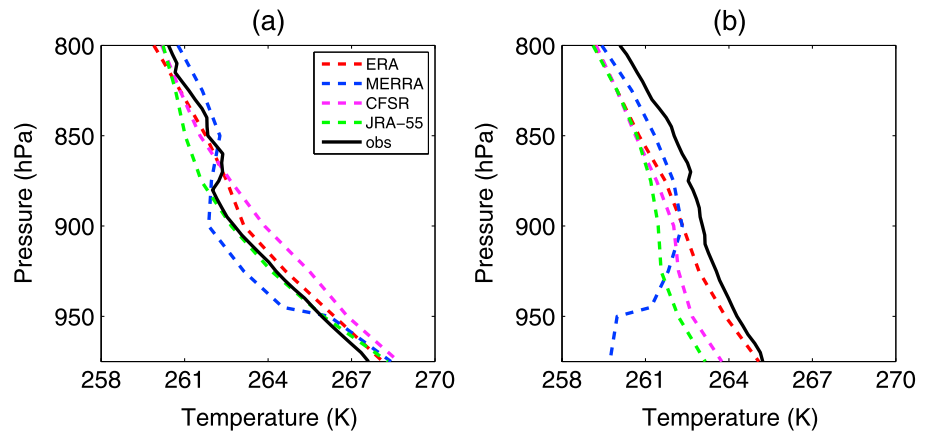


Figure 8. Radiosonde profile comparison split into two groups: (a) shelf break radiosondes (11 profiles) and (b) continental radiosondes (27 profiles). The map in Figure 1b shows the spatial split. The colored lines represent the same reanalysis products as in Figure 7.

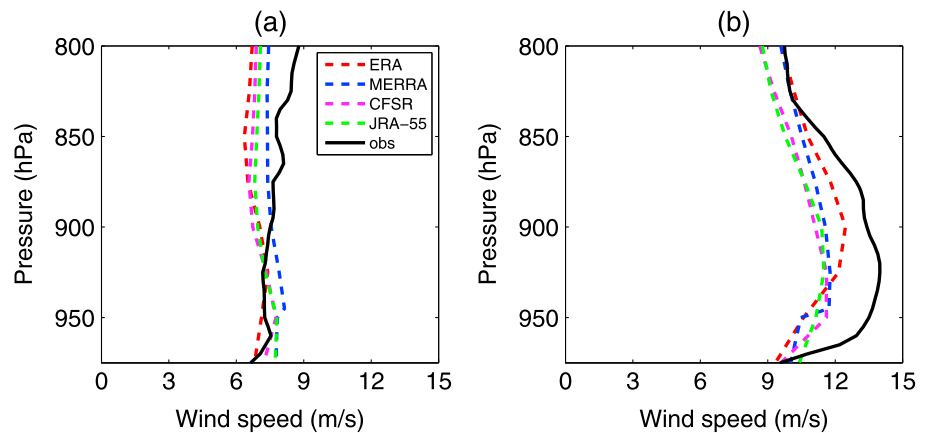


Figure 9. Average wind speed profiles split for two groups of radiosondes: (a) 17 profiles where a low level jet (LLJ) was not observed and (b) 21 profiles where a LLJ was recorded by the radiosonde. The colored lines represent the same reanalysis products as in Figure 7.

Jakobson *et al.*, 2012]. Lüpkes *et al.* [2010] show that ERA-I overestimates the altitude of the inversion base. Here individual profiles (not shown) suggest that reanalysis inversions are vertically too broad and often too weak, contributing to the larger temperature biases seen in JRA-55, CFSR, and MERRA.

4. Discussion

4.1. Common Reanalysis Traits

All four of the reanalyses generally produce lower temperatures than those observed at the AWS sites. This cold bias is also evident (to a lesser extent) over the open ocean in comparison with summertime observations from research vessels and radiosondes. Over the ocean all of the products display greater cold biases near to the coastline compared with farther out to sea, in agreement with temperature profile comparisons to the radiosondes. All the reanalyses are generally less accurate for temperature and humidity profiles closer to the continent and when there is a low-level inversion.

The AWS comparison revealed that all of the reanalysis products underestimate strong wind events ($>15 \text{ m s}^{-1}$), suggesting they struggle to capture orographic and katabatic enhancement of the winds, and they overestimate low wind speeds. The reanalyses provide an improved representation of wind speeds over the ocean, when compared with the summertime research vessel observations. They continue to show small negative biases in mean wind speed, but the systematic biases at low and high wind speeds are not seen. The reanalyses are generally less accurate for wind speed profiles when a LLJ occurs; these are typically underestimated by $2\text{--}3 \text{ m s}^{-1}$. This is consistent with Liu *et al.* [2015] where ERA-I produced LLJs that were too weak and too vertically diffuse in comparison with Arctic dropsonde data.

4.2. ERA-I Specifics

Compared with observations at the three AMRC AWS (with 3 year records), ERA-I shows the smallest cold biases of between -1.4°C and -3.0°C . These biases are similar to those found by Jones and Lister [2015] at AWS sites around the Ross Sea coastline, but they are larger than the ERA-I cold biases in coastal East Antarctica found by Bracegirdle and Marshall [2012]. ERA-I has a much larger cold bias in austral winter than summer, possibly because it is not accurately reproducing the strong surface-based inversion that is commonly observed during the polar night [King, 1990]. Generally, ERA-I has the smallest cold bias of the reanalyses examined, although JRA-55 performs slightly better in the research vessel comparison.

Relative and specific humidity biases in ERA-I are small compared with the other reanalysis products. Across the three comparisons, specific humidity biases are between -0.05 and -0.20 g kg^{-1} , while RH biases are between -1 and -6% , although the RMSE for RH is generally between 5 and 15%. The wind speed biases are typically between -0.80 and -1.40 m s^{-1} (only JRA-55 has smaller wind speed biases), and the pattern of the biases at high and low wind speeds compared with AWS observations is the same as that seen in

the other reanalyses. Overall, ERA-I contains the smallest temperature and humidity biases compared with observational data sets in the ASE, making it the most accurate product, based on this comparison.

4.3. JRA-55 Specifics

JRA-55 cold biases are somewhat larger than those seen in ERA-I but typically smaller than those in CFSR and MERRA, particularly in comparison with research vessel data. In the shelf break group of radiosonde profiles, and from the research vessel comparison, JRA-55 produces similar statistics to ERA-I for temperature over open water. JRA-55 contains the smallest biases in wind speed compared to AWS and research vessel observations. Generally, in the research vessel comparison JRA-55 is the most accurate of the reanalysis products; however, in the radiosonde profile comparisons it produces temperature and wind speed profiles with larger biases and RMSEs than ERA-I. This may be in part due to the reduced horizontal resolution of its pressure-level data. Overall, JRA-55 compares well to the in situ observations.

4.4. CFSR Specifics

Compared with AWS observations the magnitude of CFSR cold biases is relatively constant across all four seasons but larger than those seen in ERA-I and JRA-55 (e.g., Table 2 and Figure 2). Figure 3c shows that in summertime the CFSR cold bias is larger when the observed temperature is lower. Generally, the CFSR cold biases in the ASE are larger than those found in coastal East Antarctica by *Bracegirdle and Marshall* [2012]. Radiosonde cold biases are slightly larger than ERA-I but smaller than JRA-55 and MERRA. The CFSR humidity profiles are as accurate as ERA-I, producing the correct shape of both relative and specific humidity profiles. The specific humidity biases are also typically small between -0.02 and -0.22 g kg^{-1} across the three comparisons, similar to values from ERA-I. The CFSR wind speed comparison against the AWS has the largest negative bias, although the performance over the ocean is comparable to the other reanalyses.

4.5. MERRA Specifics

MERRA has the largest temperature bias of the four reanalysis products evaluated. Near-surface temperatures are colder than the AWS observations by approximately 6.8°C . This is significantly larger than the MERRA cold biases found by *Bracegirdle and Marshall* [2012] in coastal East Antarctica, which implies this large cold bias may be confined to West Antarctica. Figure 5 demonstrates that MERRA temperature biases are much larger close to the continent—a spatial pattern that is enhanced compared to the other reanalyses. Profiles suggest MERRA predicts a surface-based temperature inversion that is both stronger and more frequent than seen in the observations.

Specific humidity biases are also larger than in the other reanalysis products, with dry biases of 0.5 g kg^{-1} for the radiosonde and AWS comparisons. *Jakobson et al.* [2012] find MERRA had a similar magnitude dry bias in the lower troposphere over the Arctic, but there the magnitude of the bias increased with height rather than decreased. Overall, large temperature and humidity biases make MERRA the least accurate of the reanalysis products for the Amundsen Sea.

4.6. Implications

Overall, the reanalyses assessed here provide a reasonable estimate of the state of the atmosphere over the ASE. But while their accuracy at moderate wind speeds over open water is good, there should be some caution when wind speeds are high ($>15 \text{ m s}^{-1}$), as these high wind speeds are likely to be underestimated. Also near complex coastal topography caution should be exercised as the reanalyses are unable to adequately capture the variability in winds. For example, the research vessel (and radiosonde) RMSE is relatively large compared to other open-ocean locations [e.g., *Li et al.*, 2013; *Harden et al.*, 2015]. These shortcomings would lead to underestimates in surface wind stress during high wind speed conditions and consequently alter the wind stress curl. Errors in the wind stress and its curl would lead to errors in the dynamics of an ocean model forced by these reanalyses and will hamper the interpretation of observed ocean variability. They could also lead to an underestimate of sea ice divergence and the frequency of coastal polynyas.

The cold bias will affect both the surface sensible and latent heat fluxes, implying an overestimate in both heat fluxes (as the reanalyses are too cold and too dry). It has previously been shown that an older reanalysis product, the National Center for Environmental Prediction Reanalysis 1, contained a cold temperature bias which changed the modeled melt rates of ice shelves and ice shelf cavities in the Amundsen Sea [*Timmermann et al.*, 2012; *Nakayama et al.*, 2014]. However, the cold (and dry) bias combined with the

potential underestimation of high wind speeds may partially offset one another for the heat fluxes [e.g., Renfrew *et al.*, 2002]. Nevertheless, such errors cannot entirely compensate across a range of values, so unknown errors will be introduced. In addition, the spatial distribution of these biases may lead to an underestimation of the importance of surface fluxes near the coast where the cold biases are particularly large.

5. Conclusions

In a validation study for the Amundsen Sea Embayment, the four most recently released global meteorological reanalysis products all produce cold biases of between approximately -1.8°C (ERA-I) and -6.8°C (MERRA) when compared with year-round AWS observations. Cold biases were also found in comparisons with ship-based and radiosonde observations, although these comparisons are restricted to the summer lower troposphere. ERA-I has the smallest temperature bias. The reanalysis cold bias in coastal regions of Antarctica is in agreement with previous studies [Bracegirdle and Marshall, 2012; Jones and Lister, 2015], although these did not cover coastal West Antarctica. A seasonal comparison of the biases shows that ERA-I has the smallest temperature bias in austral summer, but all reanalysis products contain cold biases in austral winter. This implies parameterizations may perform less well during the winter months. For all the reanalysis products the magnitude of temperature biases varies spatially. Close to the ice shelves that form large parts of the ASE coastline, the cold bias is much larger than in areas more distant from the coastline. Vertical profiles from the reanalyses generally correspond better away from the coastline and in the absence of temperature inversions or low-level jets.

In the comparison to AWS wind speeds, all four reanalysis products severely underestimate when observations are above 15 m s^{-1} and overestimate when observations are below 5 m s^{-1} . Over the ocean, compared with research vessel observations, the reanalyses provide improved representation of wind speed. This is in contrast with results from Li *et al.* [2013] who found ERA-I contained the same low and high wind biases in comparison with Southern Ocean ship observations.

Overall, ERA-I has the smallest biases and errors in near-surface fields compared with meteorological observations within the ASE. This is consistent with the Antarctic-wide study of Bracegirdle and Marshall [2012]. CFSR and JRA-55 have slightly larger cold biases but have a similar level of accuracy as ERA-I in the wind speed and humidity fields. MERRA contains the largest surface temperature bias and because of this also contains a large dry bias. The large MERRA temperature bias may be spatially limited to ASE [cf. Bracegirdle and Marshall, 2012]. The biases at high and low observed wind speeds may be indicative of winds around other parts of coastal Antarctica.

Despite the use of a wide variety of meteorological data sets in this study there remains a lack of observations from West Antarctica. For example, the authors are not aware of any sustained wintertime meteorological observations over the sea ice or open water of the Amundsen Sea. Through fully utilizing the existing observations and introducing a new data set, this study provides a generally consistent evaluation of the reanalysis products in this area.

References

- Andreas, E., K. Claffy, and A. Makshtas (2000), Low-level atmospheric jets and inversions over the western Weddell Sea, *Boundary Layer Meteorol.*, 459–486.
- Assmann, K. M., A. Jenkins, D. R. Shoosmith, D. P. Walker, S. S. Jacobs, and K. W. Nicholls (2013), Variability of circumpolar deep water transport onto the Amundsen Sea continental shelf through a shelf break trough, *J. Geophys. Res. Oceans*, 118, 6603–6620, doi:10.1002/2013JC008871.
- Bracegirdle, T. J. (2013), Climatology and recent increase of westerly winds over the Amundsen Sea derived from six reanalyses, *Int. J. Climatol.*, 33(4), 843–851, doi:10.1002/joc.3473.
- Bracegirdle, T. J., and G. J. Marshall (2012), The reliability of Antarctic tropospheric pressure and temperature in the latest global reanalyses, *J. Clim.*, 25(20), 7138–7146, doi:10.1175/JCLI-D-11-00685.1.
- Bromwich, D. H., F. O. Otieno, K. M. Hines, K. W. Manning, and E. Shilo (2013), Comprehensive evaluation of polar weather research and forecasting model performance in the Antarctic, *J. Geophys. Res. Atmos.*, 118, 274–292, doi:10.1029/2012JD018139.
- Clem, K., and R. Fogt (2015), South Pacific circulation changes and their connection to the tropics and regional Antarctic warming in austral spring, 1979–2012, *J. Geophys. Res. Atmos.*, 120, 2773–2792, doi:10.1002/2014JD022940.
- Condron, A., and I. A. Renfrew (2013), The impact of polar mesoscale storms on northeast Atlantic Ocean circulation, *Nat. Geosci.*, 6, 34–37, doi:10.1038/ngeo1661.
- Deb, P., A. Orr, S. H. Hosking, T. Phillips, J. Turner, D. Bannister, J. Pope, and S. Colwell (2016), An assessment of the Polar Weather Research and Forecast (WRF) model representation of near-surface meteorological variables over West Antarctica, *J. Geophys. Res. Atmos.*, 121, 1532–1548, doi:10.1002/2015JD024037.
- Dee, D. P., et al. (2011), The ERA-Interim reanalysis: Configuration and performance of the data assimilation system, *Q. J. R. Meteorol. Soc.*, 137(656), 553–597, doi:10.1002/qj.828.

Acknowledgments

The authors appreciate the support of the University of Wisconsin-Madison Automatic Weather Station Program (via <http://amrc.ssec.wisc.edu>) for the data set, data display, and information, NSF grant numbers ANT-0944018 and ANT-1245663. Further thanks to the support team at NYU for the pre-processing and provision of data from the AWS installed on PIG, all made possible by NSF grant ANT-0732869 and NYU Abu Dhabi G1204. The JCR meteorological data and radiosonde observations will become available from the British Oceanographic Data Centre during 2016 <https://www.bodc.ac.uk>. For further information or immediate access to the radiosonde data, contact the corresponding author. The *Polarstern* meteorological data are available from the PANGAEA website <http://doi.pangaea.de/10.1594/PANGAEA.743575>. The *Palmer* meteorological data are available from http://www.marine-geo.org/tools/search/Files.php?data_set_uid=9878. The authors would also like to thank the staff at the Computational and Information Systems Laboratory research data archive for providing access to the reanalysis data sets for ERA-Interim, CFSR, and JRA-55 (via <http://rda.ucar.edu>). The Global Modeling and Assimilation Office (GMAO) and the GES DISC are acknowledged for the dissemination of the MERRA data set (via <http://disc.sci.gsfc.nasa.gov>). This work was supported by funding from the UK Natural Environment Research Council's iSTAR Programme and NERC grant number (NE/J005703/1), through a NERC funded PhD (NE/K011154/1) based at the University of East Anglia. Many thanks to iSTAR colleagues for their helpful advice and comments on this work, particularly to all science staff and crew on board JCR 294/295 for their assistance with launching radiosondes. The authors wish to thank the reviewers for their helpful comments and suggestions which have improved this manuscript.

- Ding, Q., E. J. Steig, D. S. Battisti, and M. Küttel (2011), Winter warming in West Antarctica caused by central tropical Pacific warming, *Nat. Geosci.*, *4*(6), 398–403, doi:10.1038/ngeo1129.
- Dutrieux, P., J. De Rydt, A. Jenkins, P. R. Holland, H. K. Ha, S. H. Lee, E. J. Steig, Q. Ding, P. E. Abrahamson, and M. Schröder (2014), Strong sensitivity of Pine Island ice-shelf melting to climatic variability, *Science*, *343*(6167), 174–178, doi:10.1126/science.1244341.
- Elvidge, A. D., I. A. Renfrew, J. C. King, A. Orr, and T. A. Lachlan-Cope (2016), Foehn warming distributions in non-linear and linear flow regimes: A focus on the Antarctic Peninsula, *Q. J. R. Meteorol. Soc.*, *142*, 618–631, doi:10.1002/qj.2489.
- Fogt, R. L., A. J. Wovrosh, R. A. Langen, and I. Simmonds (2012), The characteristic variability and connection to the underlying synoptic activity of the Amundsen-Bellinghshausen Seas Low, *J. Geophys. Res.*, *117*, D07111, doi:10.1029/2011JD017337.
- Genthon, C., D. Six, V. Favier, M. Lazzara, and L. Keller (2011), Atmospheric temperature measurement biases on the Antarctic plateau, *J. Atmos. Oceanic Technol.*, *28*(12), 1598–1605, doi:10.1175/JTECH-D-11-00095.1.
- Harden, B. E., I. A. Renfrew, and G. N. Petersen (2011), A climatology of wintertime barrier winds off southeast Greenland, *J. Clim.*, *24*(17), 4701–4717, doi:10.1175/2011JCLI4113.1.
- Harden, B. E., I. A. Renfrew, and G. N. Petersen (2015), Meteorological buoy observations from the central Iceland Sea, *J. Geophys. Res. Atmos.*, *120*, 3199–3208, doi:10.1002/2014JD022584.
- Hosking, J. S., A. Orr, G. J. Marshall, J. Turner, and T. Phillips (2013), The influence of the Amundsen-Bellinghshausen Seas Low on the climate of West Antarctica and its representation in coupled climate model simulations, *J. Clim.*, *26*(17), 6633–6648, doi:10.1175/JCLI-D-12-00813.1.
- Jacobs, S. S. (2014), Underway Hydrographic, Weather and Ship-state Data (JGOFs) from Nathaniel B. Palmer expedition NBP0901 (2009), Integrated Earth Data Applications (IEDA), doi:10.1594/IEDA/309878.
- Jacobs, S. S., A. Jenkins, C. F. Giulivi, and P. Dutrieux (2011), Stronger ocean circulation and increased melting under Pine Island Glacier ice shelf, *Nat. Geosci.*, *4*(8), 519–523, doi:10.1038/ngeo1188.
- Jakobson, E., T. Vihma, T. Palo, L. Jakobson, H. Keernik, and J. Jaagus (2012), Validation of atmospheric reanalyses over the central Arctic Ocean, *Geophys. Res. Lett.*, *39*, L10802, doi:10.1029/2012GL051591.
- Jones, P. D., and D. H. Lister (2015), Antarctic near-surface air temperatures compared with ERA-Interim values since 1979, *Int. J. Climatol.*, *35*(7), 1354–1366, doi:10.1002/joc.4061.
- King, J. C. (1990), Some measurements of turbulence over an Antarctic ice shelf, *Q. J. R. Meteorol. Soc.*, *116*(492), 379–400.
- Kobayashi, S., et al. (2015), The JRA-55 reanalysis: General specifications and basic characteristics, *J. Meteorol. Soc. Jpn. Ser. II*, *93*(1), 5–48, doi:10.2151/jmsj.2015-001.
- König-Langlo, G. (2010), *Continuous Meteorological Surface Measurement During POLARSTERN Cruise ANT-XXVI/3*, Alfred Wegener Institute, Helmholtz Center for Polar and Marine Research, Bremerhaven, doi:10.1594/PANGAEA.743575.
- Lazzara, M. A., G. A. Weidner, L. M. Keller, J. E. Thom, and J. J. Cassano (2012), Antarctic automatic weather station program: 30 years of polar observation, *Bull. Am. Meteorol. Soc.*, *93*(10), 1519–1537, doi:10.1175/BAMS-D-11-00015.1.
- Li, M., J. Liu, Z. Wang, H. Wang, Z. Zhang, L. Zhang, and Q. Yang (2013), Assessment of sea surface wind from NWP reanalyses and satellites in the Southern Ocean, *J. Atmos. Oceanic Technol.*, *30*(8), 1842–1853, doi:10.1175/JTECH-D-12-00240.1.
- Li, X., D. M. Holland, E. P. Gerber, and C. Yoo (2014), Impacts of the north and tropical Atlantic Ocean on the Antarctic Peninsula and sea ice, *Nature*, *505*(7484), 538–542.
- Liu, Z., A. Schweiger, and R. Lindsay (2015), Observations and modeling of atmospheric profiles in the Arctic seasonal ice zone, *Mon. Weather Rev.*, *143*(1), 39–53, doi:10.1175/MWR-D-14-00118.1.
- Lüpkes, C., T. Vihma, E. Jakobson, G. König-Langlo, and A. Tetzlaff (2010), Meteorological observations from ship cruises during summer to the central Arctic: A comparison with reanalysis data, *Geophys. Res. Lett.*, *37*, L09810, doi:10.1029/2010GL042724.
- Mastrantonio, G., V. Malvestuto, S. Argentini, T. Georgiadis, and A. Viola (1999), Evidence of a convective boundary layer developing on the Antarctic plateau during the summer, *Meteorol. Atmos. Phys.*, *71*(1–2), 127–132.
- Medley, B., et al. (2014), Constraining the recent mass balance of Pine Island and Thwaites glaciers, West Antarctica, with airborne observations of snow accumulation, *Cryosphere*, *8*(4), 1375–1392, doi:10.5194/tc-8-1375-2014.
- Mouginot, J., E. Rignot, and B. Scheuchl (2014), Sustained increase in ice discharge from the Amundsen Sea Embayment, West Antarctica, from 1973 to 2013, *Geophys. Res. Lett.*, *41*, 1576–1584, doi:10.1002/2013GL059069.
- Nakayama, Y., R. Timmermann, M. Schröder, and H. H. Hellmer (2014), On the difficulty of modeling Circumpolar Deep Water intrusions onto the Amundsen Sea continental shelf, *Ocean Modell.*, *84*, 26–34, doi:10.1016/j.ocemod.2014.09.007.
- Orr, A., T. Phillips, S. Webster, A. Elvidge, M. Weeks, S. Hosking, and J. Turner (2014), Met Office Unified Model high resolution simulations of a strong wind event in Antarctica, *Q. J. R. Meteorol. Soc.*, *140*(684), 2287–2297, doi:10.1002/qj.2296.
- Pavelsky, T. M., J. Boé, A. Hall, and E. J. Fetzer (2010), Atmospheric inversion strength over polar oceans in winter regulated by sea ice, *Clim. Dyn.*, *36*(5–6), 945–955, doi:10.1007/s00382-010-0756-8.
- Pritchard, H. D., S. R. M. Ligtenberg, H. A. Fricker, D. G. Vaughan, M. R. van den Broeke, and L. Padman (2012), Antarctic ice-sheet loss driven by basal melting of ice shelves, *Nature*, *484*(7395), 502–5, doi:10.1038/nature10968.
- Renfrew, I. A. (2004), The dynamics of idealized katabatic flow over a moderate slope and ice shelf, *Q. J. R. Meteorol. Soc.*, *130*(598), 1023–1045, doi:10.1256/qj.03.24.
- Renfrew, I. A., and P. Anderson (2002), The surface climatology of an ordinary katabatic wind regime in Coats Land, Antarctica, *Tellus A*, *463*–484.
- Renfrew, I. A., G. W. K. Moore, P. S. Guest, and K. Bumke (2002), A comparison of surface layer and surface turbulent flux observations over the Labrador Sea with ECMWF analyses and NCEP reanalyses, *J. Phys. Oceanogr.*, *32*(2), 383–400.
- Renfrew, I. A., G. N. Petersen, D. A. J. Sproson, G. W. K. Moore, H. Adiwidjaja, S. Zhang, and R. North (2009), A comparison of aircraft-based surface-layer observations over Denmark Strait and the Irminger Sea with meteorological analyses and QuikSCAT winds, *Q. J. R. Meteorol. Soc.*, *135*, 2046–2066.
- Rienecker, M. M., et al. (2011), MERRA: NASA's Modern-Era Retrospective Analysis for Research and Applications, *J. Clim.*, *24*(14), 3624–3648, doi:10.1175/JCLI-D-11-00015.1.
- Rignot, E., S. Jacobs, J. Mouginot, and B. Scheuchl (2013), Ice-shelf melting around Antarctica, *Science*, *341*(6143), 266–270, doi:10.1126/science.1235798.
- Saha, S., et al. (2010), The NCEP climate forecast system reanalysis, *Bull. Am. Meteorol. Soc.*, *91*(8), 1015–1057, doi:10.1175/2010BAMS3001.1.
- Schodlok, M. P., D. Menemenlis, E. Rignot, and M. Studinger (2012), Sensitivity of the ice-shelf/ocean system to the sub-ice-shelf cavity shape measured by NASA IceBridge in Pine Island Glacier, West Antarctica, *Ann. Glaciol.*, *53*(60), 156–162, doi:10.3189/2012AoG60A073.
- Smith, S. D. (1988), Coefficients for sea surface wind stress, heat flux, and wind profiles as a function of wind speed and temperature, *J. Geophys. Res.*, *93*(88), 15,467–15,472, doi:10.1029/JC093iC12p15467.
- Stull, R. (1988), *An Introduction to Boundary Layer Meteorology*, Kluwer Academic Publishers, Dordrecht, London.

- Suortti, T. M., et al. (2008), Tropospheric comparisons of Väisälä radiosondes and balloon-borne frost-point and Lyman- α hygrometers during the LAUTLOS-WAVVAP experiment, *J. Atmos. Oceanic Technol.*, *25*, 149–166.
- Thoma, M., A. Jenkins, D. Holland, and S. Jacobs (2008), Modelling Circumpolar Deep Water intrusions on the Amundsen Sea continental shelf, Antarctica, *Geophys. Res. Lett.*, *35*, L18602, doi:10.1029/2008GL034939.
- Timmermann, R., Q. Wang, and H. H. Hellmer (2012), Ice-shelf basal melting in a global finite-element sea-ice/ice-shelf/ocean model, *Ann. Glaciol.*, *53*(60), 303–314, doi:10.3189/2012AoG60A156.
- Turner, J., S. N. Chenoli, A. Abu Samah, G. Marshall, T. Phillips, and A. Orr (2009), Strong wind events in the Antarctic, *J. Geophys. Res.*, *114*, D18103, doi:10.1029/2008JD011642.
- Turner, J., T. Phillips, J. S. Hosking, G. J. Marshall, and A. Orr (2013), The Amundsen Sea low, *Int. J. Climatol.*, *33*(7), 1818–1829, doi:10.1002/joc.3558.